Macromolecules

Article

Microscopic State of Polymer Network Chains upon Swelling and Deformation

Anna Naumova,[†] Diana Carolina Agudelo,[‡] Marcelo A. Villar,[‡] Daniel A. Vega,[§] Juan Lopez Valentin,[∥] and Kay Saalwächter*,[†]

[†]Institut für Physik—NMR, Martin-Luther-Universität Halle-Wittenberg, Betty-Heimann-Straße 7, 06120 Halle, Germany

[‡]Department of Chemical Engineering, Planta Piloto de Ingeniería Química, Universidad Nacional del Sur, CONICET, B8002 Bahía Blanca, Argentina

[§]Department of Physics, Instituto de Física del Sur (IFISUR), Universidad Nacional del Sur, CONICET, B8002 Bahía Blanca, Argentina

[∥]ICTP-CSIC, c/Juan de la Cierva 3, Madrid 28006, Spain

ABSTRACT: We use low-resolution proton NMR to probe the chain deformation in swollen and nonlinearly deformed vulcanized rubber and end-linked PDMS networks on a microscopic level, extending earlier work focusing on uniaxial stretching and isotropic dilation upon swelling toward biaxial deformation and deformation of swollen samples. Previous studies have revealed that chain deformation in bulk samples is best described by tube models, and that chains in swollen samples deform affinely after an initial desinterspersion stage, upon which entanglement-related packing effects are relieved. We test whether a subsequent deformation may also be closer to affine, and find that this is not the case. Unexpectedly, nonisotropic deformation of swollen samples also follows tube-model predictions, which is explained by a dominance of structural inhomogeneities and significant reorganization of the topological constraints active in the swollen and possibly even the bulk state.
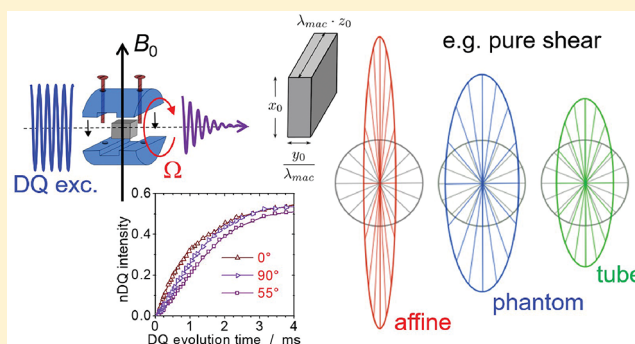
1. INTRODUCTION

Elasticity is the most important and prominent property of rubber, being able to restore its original shape after even large deformation. The restoring force in the deformed state is entropic in nature, as already concluded by William Thomson (Lord Kelvin) and James Prescott Joule in the 19th century,[1] not long after the discovery of sulfur cross-linking processes of natural rubber in 1839. Microscopic models predicting the entropy change upon deformation are abundant, with the most common ones being the two "classical" affine and phantom models, and the nonclassical tube model.[2]

The simplistic affine model equates the microscopic and macroscopic deformation, and is based upon continuum mechanics rather than a molecular concept. The phantom network model, first proposed by James and Guth,[3] remedies this shortcoming and considers cross-link fluctuations. Although the "phantom" assumption, neglecting next-neighbor packing constraints, is not quite realistic, the model was found to provide a good approximation for many experimental results,[4−6] in particular for gels and the state of equilibrium swelling.[7−10] Recent developments have focused on the effect of defects, which comprise elastically inactive components such as dangling chain ends, unentangled loops, and free chains. The amount of such defects is easily accessible in any network

by proton NMR spectroscopy.[8,11] In specific systems, network disintegration spectroscopy can be used to assess the formation of cyclic structures.[12] Upon the basis of the latter work, a new "real elastic network theory", considering the elastic effectiveness due to the defects in combination with the phantom model, has been shown to fit experimental data very well.[13,14]

Turning back to bulk samples and to effects arising from surrounding chains, Erman's constrained junction model[4] can explain experimental results that are placed in-between the phantom and affine predictions. Starting with de Gennes' reptation model[15] and the resulting tube model,[16−18] which explain the viscoelastic behavior for polymer melts arising from entanglement effects and restrictions to cross-link fluctuations, many variations of tube models were proposed for bulk as well as swollen networks.[17,19−25]

Neutron scattering is commonly taken as the standard approach to provide a microscopic probe of the macroscopic deformation, and thus to put theoretical approaches to a test. In networks, such endeavors were so far restricted to the study of the conformation of chains in end-linked model net-

works[26,27] or of labeled paths of variable length in randomly cross-linked (vulcanized) elastomers.[28] On the most local level, neutron spin echo spectroscopy[29] was used to reveal the anisotropy of entanglement constraints in lowly cross-linked stretched rubbers, confirming the applicability of a tube model. We are not aware of comparable studies in swollen and deformed gels. Without specifically labeled chains, such experiments only provide information on the correlation length (mesh size), and the scattering response is dominated by swelling heterogeneities, i.e., transient as well as frozen-in concentration fluctuations.[30,31] Even in the best available model systems, scattering features due to concentration fluctuations were reported to override information on chain stretching.[32] Therefore, advanced low-resolution proton NMR spectroscopy, namely multiple-quantum (MQ) NMR,[33,34] provides a viable alternative to study the local deformation of network chains in rubbers and gels.

Our previous NMR work was concerned with network chain deformation in isotropically swollen networks[35,36] and in uniaxially deformed bulk rubbers.[37,38] Network swelling was identified as strongly nonaffine during an initial stage up to a swelling degree $Q = V/V_0$ of order 2, during which packing and entanglement constraints are relieved. However, beyond this stage the local chain deformation was found to follow affine behavior (note that also the phantom model assumes affine deformation of average cross-link positions, and is thus compatible with the noted results obtained under isotropic dilation). Uniaxial stretching results on bulk samples were found to be most compatible with predictions of different tube models, while the affine and phantom models could be excluded.

MQ NMR relies on the anisotropy of strong proton dipole–dipole interactions among the protons.[33,39] In highly mobile systems such as low-molecular melts, these interactions are averaged out. In a polymer network, the chains are also very mobile but are restricted by the cross-links. The shorter a network chain between cross-links, the more restricted are the orientational excursions of the chain segments. Thus, even if the segmental time scale is too fast to exert any measurable effect, a very low local degree of anisotropy remains and can be measured very accurately by MQ NMR in terms of a residual dipolar coupling D_{res}. It contains information about the ratio between the end-to-end distance and the contour length of the given chain between constraints. D_{res} is an average quantity reflecting motional anisotropy of any given chain segment. Since its distribution can also be assessed, the results provide a rich picture of the variations of local stretching in a potentially inhomogeneously deformed sample.

For this reason, the MQ NMR method avoids some of the ambiguities arising from other NMR approaches such as the measurement of quadrupolar splittings of labeled probe molecules or network chains.[6,40–43] Similar to strain birefringence data,[44] most of these earlier works confirmed adherence to a simple affine prediction, mainly because the spectral response (i.e., the observed quadrupolar splitting) is dominated by freely diffusing species subject to nematic interactions.[45,46] The effect thus reflects average chain orientation rather than local stretching.[37]

Arguably, a wider range of different modes of deformation, including compression and biaxial strain, provides a more stringent test of elasticity theories. Along this line, Urayama concluded that the tube models available for his work cannot correctly reproduce mechanical properties.[24] More recent

computer simulations also suggest even weaker than predicted local deformation of the entanglement tube in gels made from entangled rings.[47] Therefore, herein we use MQ NMR to investigate microscopic stretching of polymer chains during anisotropic swelling and different modes of deformation of dry as well as swollen polymer networks of different chemical makeup. The main focus is on a comparison of chain deformation in the dry and partially swollen states, where for the latter affine behavior was found upon isotropic dilation by approaching swelling equilibrium. Would the chains thus be stretched affinely upon mechanical load in a preswollen sample? We will show below that this is not the case, and will discuss the implications of this finding.

2. EXPERIMENTAL SECTION

2.1. Samples. Following earlier work, we have investigated three different polymer network types, NR (natural rubber, SMR-CV60 by Malaysian Rubber), and BR (butadiene rubber (98% cis) from Polimeri Europa), both vulcanized with sulfur and peroxide,[7,48] and PDMS (telechelic vinyl-modified poly(dimethylsiloxane), United Chemical Technology, Inc.), end-linked by hydrosilylation using 3- and 4-functional cross-linkers.[49] The recipes of the samples are given in Tables 1, 2, and 3, respectively. For PDMS, the cross-linker functionality f is part of the sample name. The NMR results for this set of new samples were in good agreement with the results for a set of samples investigated earlier.[49] In addition, we have also included experiments on older end-linked PDMS samples: PDMSo-f4-58k and PDMSo-f3.6-5k from refs 50 and 51, respectively.

Table 1. Sulphur-Cured[a] Rubbers Vulcanized at 150 °C

sample	sulfur (phr)	CBS (phr)	cure time (t_{97}/min)	$D_{avg}/2\pi$ (Hz)	σ/D_{avg}	defects (%)
NR-1.3	1.3	0.26	17.91	130	0.25	8
NR-3.1	3.1	0.62	14.04	240	0.10	4
NR-7.4	7.4	1.48	11.46	450	0.15	1
BR-1.3	1.3	0.26	94.29	170	0.40	17
BR-3.1	3.1	0.62	35.07	280	0.30	7
BR-7.4	7.4	1.48	27.20	430	0.28	2

[a]Amounts of sulfur and N-cyclohexyl-2-benzothiazole sulfenamide (CBS) are given in parts per hundred rubber (phr). ZnO and stearic acid contents was 5 and 2 phr, respectively.

Table 2. Peroxide-Cured Rubbers Vulcanized at 150 °C

sample	DCP (phr)	cure time (t_{97}/min)	$D_{avg}/2\pi$ (Hz)	σ/D_{avg}	defects (%)
NR-DCP0.5	0.5	130	120	0.1	13
NR-DCP1.0	1.0	114	160	0.1	8
NR-DCP1.5	1.5	110	200	0.1	6
NR-DCP2.0	2.0	106	240	0.16	5
NR-DCP3.0	3.0	104	300	0.23	4
BR-DCP0.045	0.045	152	170	0.34	14

Table 3. PDMS Networks End-Linked with Variable Average Crosslinker Functionality (-f...-) and Precursor Molecular Weight

sample	M_n (kg/mol)	M_w/M_n	$D_{avg}/2\pi$ (Hz)	σ/D_{avg}	defects (%)
PDMSo-f4-58k	47.2	1.9	170	0.22	4
PDMS-f3-8k	7.9	2.8	190	0.28	7
PDMS-f4-8k	7.9	2.8	250	0.33	6
PDMSo-f3.6-5k	4.8	2.0	250	0.47	4

2.2. NMR Spectroscopy. All experiments were performed on three different mq20 BRUKER minispec low-field NMR instruments using sample tubes of 10 mm outer and 8 mm inner diameter. The length of the 90° pulses for these spectrometers were 1.5 μs, 2.5 μs, and 2.8 μs, and the receiver dead times were of the order of 10−15 μs.

Multiple-quantum (MQ) NMR experiments were conducted using the improved[33,50] pulse sequence of Baum and Pines[52] to probe the time evolution of mainly double-quantum (DQ) coherences in deformed rubber samples. With suitable phase-cycling and data analysis procedures,[33,34,50] involving quantification and subtraction of a slowly relaxing signal tail associated with network defects, the experiment provides a DQ build-up curve $I_{DQ}(\tau_{DQ})$ and a sum multiple-quantum decay curve $I_{\Sigma MQ}(\tau_{DQ})$ measured as a function of DQ evolution time τ_{DQ}. Using these signal functions, long-time relaxation effects (related to the time scale of segmental fluctuations) are removed from the data by point-by-point normalization, providing a normalized DQ (nDQ) build-up curve: $I_{nDQ}(\tau_{DQ})=I_{DQ}(\tau_{DQ})/I_{\Sigma MQ}(\tau_{DQ})$. This signal function provides a direct measure of residual dipolar couplings D_{res}. Results of analyses of all samples in the unswollen and unstretched bulk state are included in Tables 1−3.

2.3. Deformation of Dry and Swollen Rubber. Using different custom-made fixtures, we compared several types of deformation for dry and swollen polymer networks: uniaxial stretching, uniaxial compression, and pure-shear deformation. In addition, we performed swelling of uniaxially stretched samples, and anisotropic swelling along a single axis (uniaxial swelling). In order to exclude effects of sample aging/degradation, or slow relaxation in the case of lowly cross-linked networks, we have measured several samples repeatedly over the course of 1−2 days, thus making sure that the results are representative of equilibrated samples.

2.4. Deformation of Dry Rubber. The strain matrix for the case of uniaxial deformation is written as follows:

$$\Lambda_{uni} = \begin{pmatrix} \lambda_x & 0 & 0 \\ 0 & \lambda_y & 0 \\ 0 & 0 & \lambda_z \end{pmatrix} = \begin{pmatrix} \dfrac{1}{\sqrt{\lambda_{mac}}} & 0 & 0 \\ 0 & \dfrac{1}{\sqrt{\lambda_{mac}}} & 0 \\ 0 & 0 & \lambda_{mac} \end{pmatrix}$$

(1)

where $\lambda_{mac} = L_z/L_{z,0}$ is the macroscopic sample deformation along the z axis (being >1 or <1 for stretching or compression, respectively). For the experimental realization of uniaxial stretching we followed our previous work,[38] cutting rubber rings out of 2 mm thick sheets having different diameters (inner diameter d_1, outer diameter d_2) and rim width ($c = d_2 − d_1$). A few rings were then elongated and stripped side by side onto a thin ceramic plate with 9.5 mm width, 0.34 mm thickness and a resulting perimeter L of 19.7 mm. The macroscopic elongation (λ_{mac}) averaged over the ring width is thus,

$$\lambda_{mac} = \frac{L\left[\frac{1}{d_1} - \frac{1}{d_2}\right]}{\pi \ln(d_1/d_2)}$$

(2)

This assembly was attached to a Teflon rod connected to a computer-controlled servo motor (MSR 0020/L2-45-0, Mattke AG, Freiburg, Germany), and lowered into the NMR probe, thus controlling the angle Ω between the stretching direction and the B_0 field.

For uniaxial compression with $\lambda_{mac} < 1$, strips of rubber with initial thickness $d = 2$ mm and appropriate width were elongated in excess using a homemade stretching device and placed between two parts of a cylindrical tool as shown in Figure 1.[37] To realize different deformations, Teflon strips of variable thickness were used to adjust the final thickness after sample expansion following screw assembly and release of external strain. Sample pieces protruding from the tool were cut away.

For pure-shear deformation, where in one dimension (here: x) the sample is constrained to its original width, we have an effectively biaxial deformation as follows:
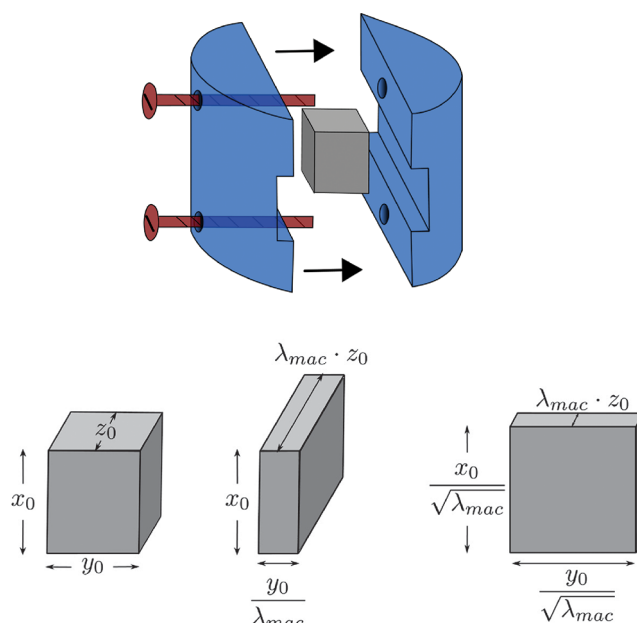
Figure 1. Compression tool with ca. 8 mm diameter fitting into a standard 10 mm NMR tube, along with a sketch of the original sample dimensions (left), and after pure-shear deformation (middle) and uniaxial compression (right).

$$\Lambda_{ps} = \begin{pmatrix} 1 & 0 & 0 \\ 0 & \dfrac{1}{\lambda_{mac}} & 0 \\ 0 & 0 & \lambda_{mac} \end{pmatrix}$$

(3)

This deformation is also easily realized with the given tool by adjusting the width and final height of the strips accordingly.

2.5. Deformation of swollen rubber. We now address the different types of deformation involving a solvent, independent of the order of swelling and external deformation. Unrestricted swelling results in isotropic dilation following

$$\Lambda_{is} = \begin{pmatrix} \sqrt[3]{Q} & 0 & 0 \\ 0 & \sqrt[3]{Q} & 0 \\ 0 & 0 & \sqrt[3]{Q} \end{pmatrix}$$

(4)

where $Q = V_{sw}/V_{dry}$ is the volumetric degree of swelling, which we have determined gravimetrically (neglecting small density differences, as the associated error is smaller than the overall accuracy). Toluene is a good solvent for all types of samples (NR, BR, and PDMS) and is available in deuterated form, proving useful for our previous swelling studies.[36] For most of our experiments on swollen and deformed samples, it was however too volatile, so we resorted to using dibutyl sebacate (DBS) and cyclohexanone, which are less volatile. However, the comparably large solvent signal in these cases, increasing the tail fraction to be subtracted during data analysis, posed stronger limitations on the accuracy of the measured data.

Combining isotropic swelling with uniaxial deformation, and assuming the Poisson ratio to be constant, the deformation matrix reads as follows:

$$\Lambda_{uni,is} = \begin{pmatrix} \sqrt[3]{Q} \times \dfrac{1}{\sqrt{\lambda_{mac}}} & 0 & 0 \\ 0 & \sqrt[3]{Q} \times \dfrac{1}{\sqrt{\lambda_{mac}}} & 0 \\ 0 & 0 & \sqrt[3]{Q} \times \lambda_{mac} \end{pmatrix}$$

(5)

This is relevant for swelling experiments on prestretched rubber samples, which we realized by immersion of the stretched-ring assembly in DBS for 10 min. This experiment usually had to be performed several times, because very often individual rings broke during the experiment. Such runs were discarded. This is also the reason why the immersion time was limited to 10 min, restricting the upper limit for Q to a value of 1.8., i.e., below swelling equilibrium. This means that the interesting data range above Q of about 2 (the affine range of isotropic swelling) was not accessible in this way.

An extended range of deformation could be accessed by uniaxial compression of preswollen rubber, which is also described by eq 5. For this experiment we compressed a swollen specimen in the tool shown in Figure 1 without restricting the sample perpendicular to the axis of compression. Pure shear could also be realized in this way, simply by matching the x lateral dimension of the swollen sample and the width of the tool. Correspondingly,

$$\Lambda_{ps,is} = \begin{pmatrix} \sqrt[3]{Q} \times 1 & 0 & 0 \\ 0 & \sqrt[3]{Q} \times \dfrac{1}{\lambda_{mac}} & 0 \\ 0 & 0 & \sqrt[3]{Q} \times \lambda_{mac} \end{pmatrix} \qquad (6)$$

Finally, uniaxial swelling proved to be a feasible strategy to realize an even larger effective deformation of swollen samples, with the possibility of even using deuterated toluene as solvent. In this case the expansion equals the degree of swelling Q along one axis,

$$\Lambda_{us} = \begin{pmatrix} 1 & 0 & 0 \\ 0 & 1 & 0 \\ 0 & 0 & Q \end{pmatrix} \qquad (7)$$

We performed this experiment by fitting sample discs of ca. 2 mm thickness and 3 mm diameter into the center of Teflon tubes of 8 mm length and 3 mm inner diameter, and immersing in deuterated toluene for several days until the networks' size reached roughly the length of the tube. The sample was then transferred to a regular 10 mm glass tube and flame-sealed. Due to the very slow kinetics and the given geometry limitations, the resulting degree of swelling was again below equilibrium, and could only be determined very approximately. For all samples, it was $Q \approx 3.5 \pm 0.5$.

3. METHODOLOGICAL BACKGROUND

The NMR response of the protons in a network far above the glass transition is dominated by the through-space dipole–dipole interaction, which is distance- as well as orientation-dependent. Since the distances of next-neighbor couplings are essentially fixed by the chemical makeup, the main influencing factor is the orientation dependence of the interaction frequency $\omega_{res}(\theta')$ following the second Legendre polynomial, $\omega_{res}(\theta') = D_{eff}P_2(\cos\theta')$, where θ' is the orientation of the segment with respect to the magnetic field, and D_{eff} is an effective "static-limit" coupling constant. The latter is taken to include preaveraging due to motions within a Kuhn segment, which are typically associated with the α process related to the glass transition. Changes of θ' in time that are fast as compared to the inverse D_{eff} (i.e., about 10 μs) lead to the observation of an averaged coupling $\omega_{res}(\theta) = D_{res}P_2(\cos\theta)$, that reports on the extent of orientational fluctuations. θ is now the orientation of the symmetry axis of motion, i.e., the end-to-end vector $\boldsymbol{R}$ of a polymer chain between constraints.

By means of the MQ NMR technique, we can not only measure the average D_{res} of polymer network chains, but also assess its distribution in case of an inhomogeneous response (i.e., the rotational mobility of different segments in different network chains can be expected to be different). D_{res} is proportional to the average dynamic order parameter of the backbone (S_b):

$$D_{res} = D_{eff} \times S_b \qquad (8)$$

For isotropic samples such as liquids, $S_b = 0$, while for frozen-in chain motion $S_b = 1$. For a Gaussian chain at fixed end-to-end distance, S_b is proportional to the end-to-end distance R:[53]

$$S_b = \frac{3}{5N}\left(\frac{R^2}{R_0^2}\right) \qquad (9)$$

where $R_0 = N l^2$ is unperturbed melt-state value, and N is the number of Kuhn segments. Thus, $S_b = 0$ for a chain whose ends are at the same point, i.e., when the end-to-end distance is zero ($R = 0$). If the chain is fully stretched, $S_b = 1$.

Combining eqs 8 and 9 leads to the correlation between D_{res} and the conformational statistics of the chain:

$$D_{res} = D_{eff} \times \frac{3}{5N}\left(\frac{R^2}{R_0^2}\right) \qquad (10)$$

For undeformed network, D_{res}, being a coupling constant, is the same for all spatial orientations of the sample with respect to the permanent magnetic field $\boldsymbol{B}_0$, but the mentioned orientation dependence $\sim P_2(\cos\theta)$ arises for the spectral splitting related to this tensorial interaction (θ being the angle between $\boldsymbol{R}$ and $\boldsymbol{B}_0$) for the differently oriented network chains. The orientation distribution is isotropic, and is implicitly considered in the data analysis ("powder average").

When the sample is stretched, however, the MQ NMR response is dependent on the orientation *of the sample* with respect to $\boldsymbol{B}_0$.[37,38] In Figure 2a, we illustrate this with nDQ build-up curves (reflecting the magnitude of D_{res}) for NR which was uniaxially stretched to a strain $\lambda = 4.1$ ($\lambda = L/L_0 = 1 + \epsilon$). The unique orientation angle Ω is here defined as the angle between the stretching axis and $\boldsymbol{B}_0$; $\Omega = 0°$ refers to the elongation axis being along $\boldsymbol{B}_0$.

The faster the experimental build-up curve is increasing, the higher is the fitted value for D_{res}. For example in Figure 2a, data for the sample orientation at $\Omega = 55°$ (green squares) has a lower slope than data for $\theta = 0°$ (red up triangles). This means that the apparent $D_{res}(0°) > D_{res}(55°)$.

To compare MQ NMR data of a stretched sample with data of an undeformed one, we can first calculate an artificially powder-averaged signal for the stretched sample,[38]

$$I_{nDQ}(\lambda \neq 1) = \frac{\sum_{\theta=0°}^{90°} I_{nDQ}(\theta) \times \sin(\theta)}{\sum_{\theta=0°}^{90°} \sin(\theta)}$$

for each point τ_{DQ} along the build-up curve. The theoretical form of the single-orientation build-up function $I_{nDQ}(\theta)$ is addressed in the next section. Figure 2b shows data for an unstretched sample in comparison with such powder-averaged data for the stretched state including fits.

Using Tikhonov regularization,[54,55] one can not only obtain an averaged D_{res} value, D_{avg}, but also the width and shape of the full distribution. The stretched sample not only has a higher D_{avg} value, but also a much larger distribution width. We quantify it by the dimensionless ratio σ/D_{avg}, where σ is the numerically calculated standard deviation from the average. Its increase indicates a pronounced inhomogeneity among the chains in the stretched sample.
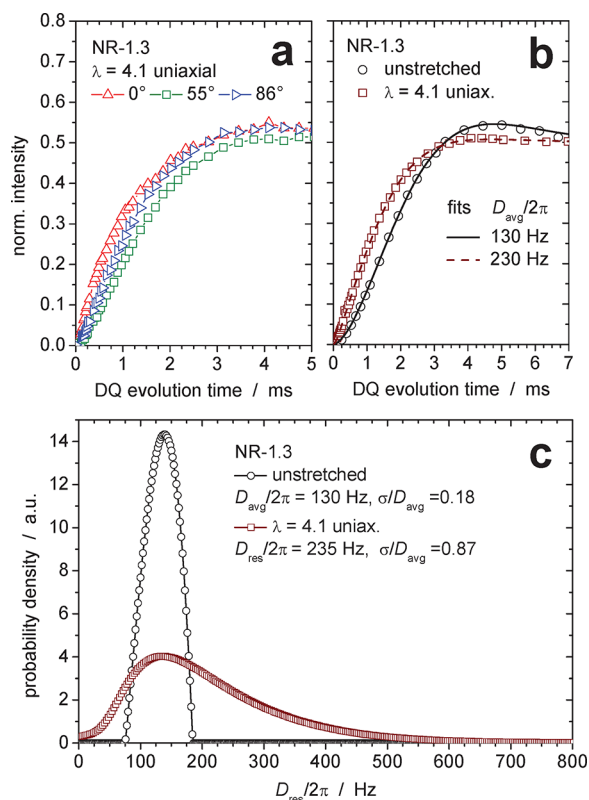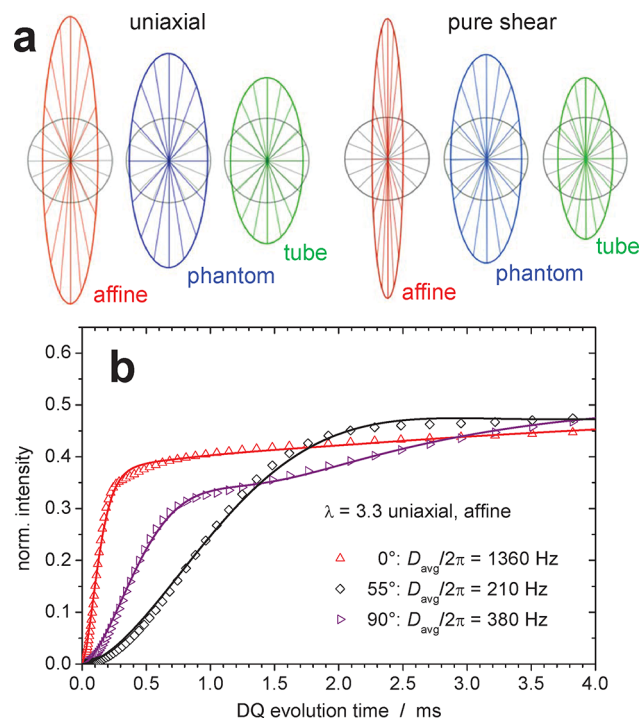
Figure 2. Experimental nDQ build-up curves for sample NR-1.3 with elongation $\lambda = 4.1$ (a) for three different orientations Ω and (b) of the artificial powder average, as compared to the unstretched case, along with (c) the distribution of residual couplings D_{res} as obtained by regularization (the lines shown in (b) correspond to these fits). Averages D_{avg} and normalized standard deviations σ/D_{avg} are given.

Figure 3. (a) "Spokeswheel" representations (plane projections) of different deformation modes for the three considered elasticity models (for pure shear the $\{\lambda,1/\lambda\}$ plane is shown). (b) Fitting of simulated nDQ build-up curves for three sample orientations Ω in affine deformation; the resulting average apparent residual couplings are indicated.

As it is obvious from Figure 2c, the higher the deformation, the more inhomogeneous and more angle-dependent the response becomes. This is actually expected, and can be rationalized by different deformation for network chains that are differently oriented with respect to the stretching direction. This is visualized by the "spokeswheel" representation shown in Figure 3a,[37] where the spokes are end-to-end vectors of representative network chains combined to originate from a common origin. Obviously, upon uniaxial deformation chains oriented along the stretching direction become elongated most, while a significant fraction is even compressed. The compressed chains correspond to the low-D_{res} range of the distributions where D_{res} is even smaller than in the original unstretched sample. This phenomenon thus explains the strong angle dependence of D_{avg} fitted to a single nDQ build-up curve measured at a given angle Ω. The background of these fits and the associated model predictions are addressed in the following section.

4. THEORY AND MODELING OF DEFORMATION

We now partially review our previous work,[37] extend our previous treatment to multiaxial deformations, and include an improved analysis method based upon model calculations using a new generic nDQ build-up function for oriented chains.[56]

In order to analyze the experimental data, we need to calculate nDQ build-up curves, for which we assume different microscopic deformations that are specific for different elasticity models. We then compare the calculated NMR data for specific models with experimental data. This involves a number of simplifying assumptions, such as that networks are free of elastically inactive defects and that all chains have the same length. The latter assumption is corroborated by the narrow D_{res} distributions found in the unstretched state; this apparent uniformity mainly arises from local force balances rather than actually equal lengths.[37,39]

We work on the basis of end-to-end vectors representing the orientation and the state of stretching of the network chains between cross-links. We rely on eq 10, which states that the residual coupling entering the build-up curve calculation is proportional to the order parameter for the given chain, and thus proportional to the end-to-end distance. The signal function is thus obtained as a sum of signals from every chain:

$$I_{nDQ}(\tau_{DQ}) = \frac{1}{N}\sum_{i=1}^{N} I_{nDQ}^{soAl}(\tau_{DQ}, D_{res,0} \times R_i^2, \theta_i) \tag{11}$$

where R_i and θ_i are the end-to-end vector for chain number i and the angle between R_i and the external magnetic field B_0, respectively. The modulus of R_i is taken to be unity in the unstretched state. We use our recently developed[56] generic orientation-dependent build-up function:

$$I_{nDQ}^{soAl}(\tau_{DQ}, D_{res}, \theta) = 0.5(1 - \exp[-\{0.455\omega_{res}(\theta)\tau_{DQ}\}^2])$$
$$\times \cos[1.86\omega_{res}(\theta)\tau_{DQ}] \tag{12}$$

the so-called "single-orientation Abragam-like" function, where $\omega_{res}(\theta) = D_{res}P_2(\cos\theta)$. Its powder average reproduces the Abragam-like build-up function that we use for analysis of isotropic samples.[55] Generally, these functions provide very

good descriptions of elastomers or liquid crystals with many protons close to the molecular backbone, and fast, effectively uniaxial dynamics. D_{res} represents a second-moment-type quantity, reflecting a multispin coupling situation dominated by dipolar truncation.[34]

Data for stretched samples are complex because the signal from every chain depends not only on the length of the chain, but also on the orientation of the chain with respect to the B_0 field. This means that these two variables cannot be analyzed separately. In our calculations, we have used 100 000 chains to represent the network. In the network, all orientations are present and the initial orientation distribution in the underformed state is isotropic. We realize this by an even, random orientation distribution of points on a unit sphere. The application of eqs 11 and 12 thus provides the regular powder average.

The calculation for a stretched sample is performed using the same set of vectors R_i with their respective orientation θ_i, but after applying a transformation following different model predictions. In this work we have examined three models of rubber elasticity: the two classical models (affine and phantom) and the nonaffine tube model,[22,23] all of which have been tested already in our previous work.[37]

Figure 3a showns a visual representation of the microscopic deformations of chains calculated for the different models in uniaxial deformation and pure shear. We recapitulate the details concerning the microscopic deformation only for the former. In case of the simple **affine model**, the local deformation matrix is identical the macroscopic one, i.e.,

$$\Lambda_{loc,uni}^{affine} = \Lambda_{mac,uni} \tag{13}$$

The **phantom model** takes into account junction fluctuation as constrained by the attached chains, yet chains are assumed to be noninteracting with surrounding chains and are even allowed to cross each other. This results in a less-than-affine local deformation,[57,58]

$$\Lambda_{loc,uni}^{phantom} = \begin{pmatrix} \sqrt{\dfrac{1+\lambda_{mac}}{2\lambda_{mac}}} & 0 & 0 \\ 0 & \sqrt{\dfrac{1+\lambda_{mac}}{2\lambda_{mac}}} & 0 \\ 0 & 0 & \sqrt{\dfrac{1+\lambda_{mac}^2}{2}} \end{pmatrix} \tag{14}$$

The nonaffine **tube model** considered here[22,23] assumes the diameter of the constraining tube to be proportional to deformation. This results in a microscopic deformation is as follows:

$$\Lambda_{loc,uni}^{tube} = \begin{pmatrix} \dfrac{1}{\sqrt[4]{\lambda_{mac}}} & 0 & 0 \\ 0 & \dfrac{1}{\sqrt[4]{\lambda_{mac}}} & 0 \\ 0 & 0 & \sqrt{\lambda_{mac}} \end{pmatrix} \tag{15}$$

We should also comment on the **molecular stress function model** (MSFM), another special tube-model variant[58] that was also tested in our previous work.[37] This model was found to fit

experimental data about as good as or even better than the tube model, mostly with respect to the angle dependence. However, the latter was studied rather qualitatively, focusing on changes in nDQ intensity for a given very short evolution time (initial-rise approximation). These data turned out to be rather biased as compared to the more quantitative modeling and fitting procedure described herein, which provides a more reliable average. Within the new approach, the predictions from both models are rather similar. Therefore, we excluded the MSFM.

In Figure 3b we show calculated meta-data for uniaxial stretching ($\lambda = 3.3$) and affine behavior. The nDQ build-up curves demonstrate nontrivial shape changes for different sample orientations Ω. These are not reproduced in experimental data on real, less ideal networks (see Figure 2a). So in order to compare such results for different models with experiments, we focus on the angular dependence of an average apparent D_{avg} that we fit to the angle-dependent curves using the same numerical regularization procedure normally used for isotropic samples.[55] Corresponding results for fits to meta-data from model predictions are also displayed in Figure 3b. These fits are subject to an ambiguity related to the fitted data range of τ_{DQ} arising from the long-time oscillations in such relaxation- and noise-free data, resulting in an uncertainty of the obtained D_{avg} of approximately 10%. This leads to some "noise" in the simulated data for $D_{avg}(\Omega)$. In the following, we quantify the orientation and stretching effects via the normalized quantity $D_{avg}(\Omega)/D_{avg}(\lambda = 1)$.

5. RESULTS AND DISCUSSION

We first illustrate the principle of our experiments by confirming results from our previous works concerned with bulk uniaxial stretching[37] and isotropic swelling[36] on our new samples, see Figure 4a and b, respectively. For bulk deformation, the left panel in Figure 4a shows D_{res} distributions for different elongations λ, which are obtained from quasi-isotropic nDQ build-up curves combined from measurements at various orientations Ω. These highlight the increasing broadening of the distribution dominated by the orientation-dependent chain stretching, see Figure 3a. D_{avg} values obtained from these distributions, normalized to the D_{res} value for the unstretched sample, are plotted vs λ in the right panel, where they are compared with different model predictions. We confirm that these data are best described by the tube model, in particular at larger λ, while the phantom model seems to work better for smaller elongation.

Swelling has an even more pronounced effect on the D_{res} distribution, see the left panel of Figure 4b.[35] While a large fraction of chains appear to be relaxed, only a minority fraction is strongly stretched and carries the elastic load. The significant width of these distributions poses limitations on the data quality of the D_{avg} values derived from these distributions, see the right panel. At low Q, D_{avg} is first decreasing (desinterspersion of entanglements) and then increasing upon further swelling up to equilibrium.[36]

In the first stage entanglements are diluted[49] and junction fluctuations are modified accordingly;[59] a detailed description of this process is subject to ongoing work. Empirically, we observe a nearly affine deformation beyond $Q \approx 2.5$, where $D_{res} \propto R^2 \propto Q^{2/3}$. This was demonstrated earlier and with better statistics for a larger variety of samples.[36] The affine back-extrapolation was shown to provide an estimated measure of the true chemical cross-link density (plus residual entangle-
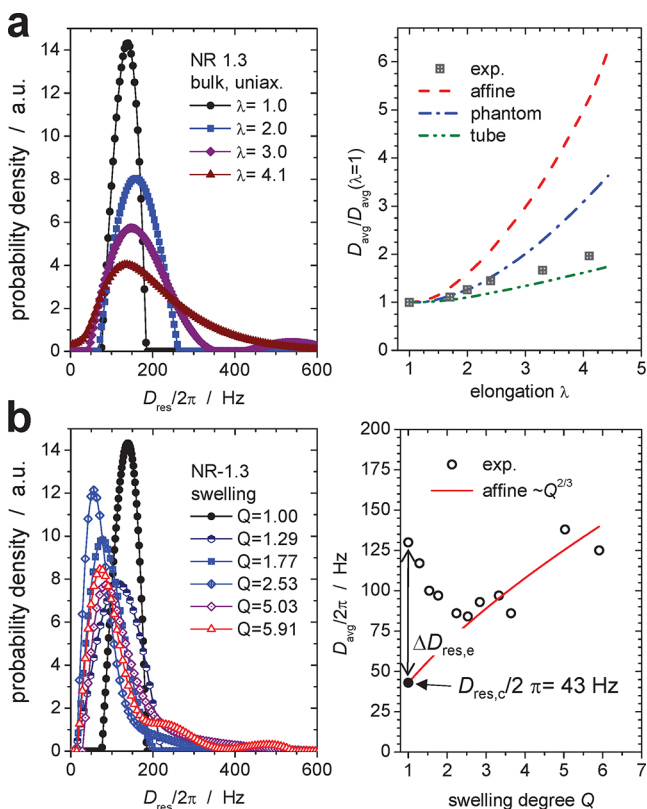
Figure 4. D_{res} distributions (left) and deformation-dependent average couplings D_{avg} (right) for sample NR-1.3 for (a) uniaxial elongation in bulk and (b) isotropic dilation upon swelling in cyclohexanone. In (a) predictions for the three considered models are shown, while in (b) the back-extrapolation assuming affine deformation for late-stage swelling is shown along with the derived contributions from cross-links ($D_{res,c}$) and entanglements $\Delta D_{res,e}$.

Table 4. Entanglement Molecular Weights[61] and Corresponding as Well as Experimental $D_{res,e}$ Values for Polymers Used in This Work

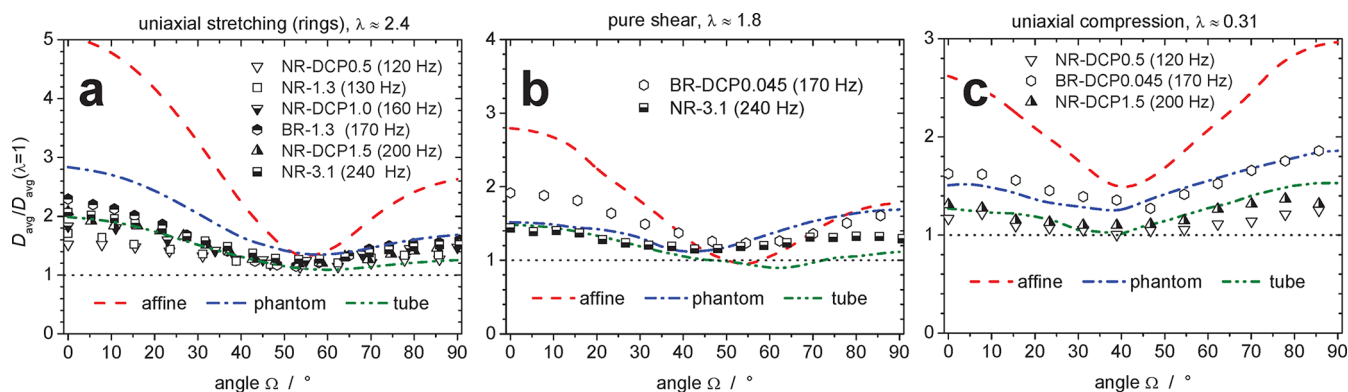| polymer	M_e (kg/mol)	calc. $\Delta D_{res,e}/2\pi$ (Hz)		exp. $\Delta D_{res,e}/2\pi$ (Hz)	
		$f = 4$	$f = 3$	$f = 4$	$f = 3$
NR	3.9	80		115 ± 20	
cis-BR	~2.9	110		90 ± 10	
PDMS	12.0	50	35	80 ± 10	70 ± 10

and across different samples, the agreement between experimental and predicted trends is satisfactory. Comparing the given $\Delta D_{res,e}$ values with the bulk results for D_{avg} in Tables 1−3 shows that only the lowest-cross-linked of our samples are entanglement-dominated, while all others feature a dominant contribution of actual cross-links.

5.1. Deformation of Dry Networks: Uniaxial Stretching, Uniaxial Compression and Pure Shear. The angular dependencies of the normalized D_{avg} for 3 different types of deformation are collected in Figure 5a−c, where in each case various samples are compared for a given value of λ. Generally, since $D_{res} \propto R^2$, we expect that a larger elongation of end-to-end distances R at stronger deformation leads to a stronger angular dependency and higher values of D_{avg}. For uniaxial stretching (Figure 5a) at angle $\Omega = 0°$ we observe quite some variation from 1.5 to 2.3 across the sample series. This range seems to be correlated with cross-linking density for the NR series, irrespective of the cross-linking chemistry (sulfur vs DCP). The trend could be interpreted as a transition from tube- to cross-link-dominated behavior. We stress that sulfur-cross-linked NR tends to degrade over time in swollen samples when exposed to light and ambient oxygen,[7] yet such effects are proven to be absent by way of our sample variations.

BR in turn with similar cross-linking density as NR shows a significantly larger angular dependency. In other words, chains in BR appear to be more stretched than in NR. Since the entanglement contributions in all these samples $\Delta D_{res,e}$ are similar in both series, the difference cannot be due to entanglement effects. A higher D_{avg} for BR in comparison to NR is also noticeable for pure shear deformation (Figure 5b) and uniaxial compression (Figure 5c). Rationalizing this difference appears difficult, and we hypothesize that it may be due to subtle differences in the topology and/or the spatial cross-link distribution on these samples, which is not apparent in the undeformed bulk but only unfolds in the nonlinear regime.

Comparing the data with the three different predictions for all three deformation types, we can again conclude that the tube model provides the overall best description of the data. For an alternative interpretation, we plot in Figure 6 orientation-dependent data for two NR samples, in each case fitted to match one of the three elasticity models by assuming a variable fraction of actually deformed chains coexisting with undeformed chains. This approach is seen to provide a similarly good fit for each of the models, with some preference for the phantom model. The possibility of such inhomogeneous response will be further highlighted in the context of swollen samples, to be addressed in the following section.

5.2. Deformation of Swollen Networks. There are three different options to combine anisotropic mechanical deformation and swelling of rubber, (i) swelling of predeformed rubber, (ii) deformation of swollen rubber, (iii) and

ment effects that are active in the swollen state), and its difference to D_{avg} of the bulk sample, $\Delta D_{res,e}$, quantifies the main contributions from entanglements and other packing-related constraints in the dry samples. This is illustrated in Figure 4b, right panel.

In order to compare D_{res} values and their relation to the cross-link densities of different polymers, we need to consider their dependence on the molecular weight of the network chains (M_c), as previously worked out for NR,[7,60] BR,[48,60] and PDMS,[8,60]

$$M_c^{NR} = \frac{617 \text{Hz}}{D_{res}/2\pi} \times \frac{f-2}{f} \quad (\text{kg/mol}) \qquad (16)$$

$$M_c^{BR} = \frac{656 \text{Hz}}{D_{res}/2\pi} \times \frac{f-2}{f} \quad (\text{kg/mol}) \qquad (17)$$

$$M_c^{PDMS} = \frac{1266 \text{Hz}}{D_{res}/2\pi} \times \frac{f-2}{f} \quad (\text{kg/mol}) \qquad (18)$$

where f is cross-link functionality. These conversion factors depend on a model and rather simplifying assumptions,[60] but have been shown to be accurate within about 30%.[7,8,48] We use these relations here only to compare the entanglement-related contribution $\Delta D_{res,e}$ predicted from these relations with experimental results from the extrapolation procedure discussed above. This comparison is summarized in Table 4. Given the relatively large scatter for the data of a given sample
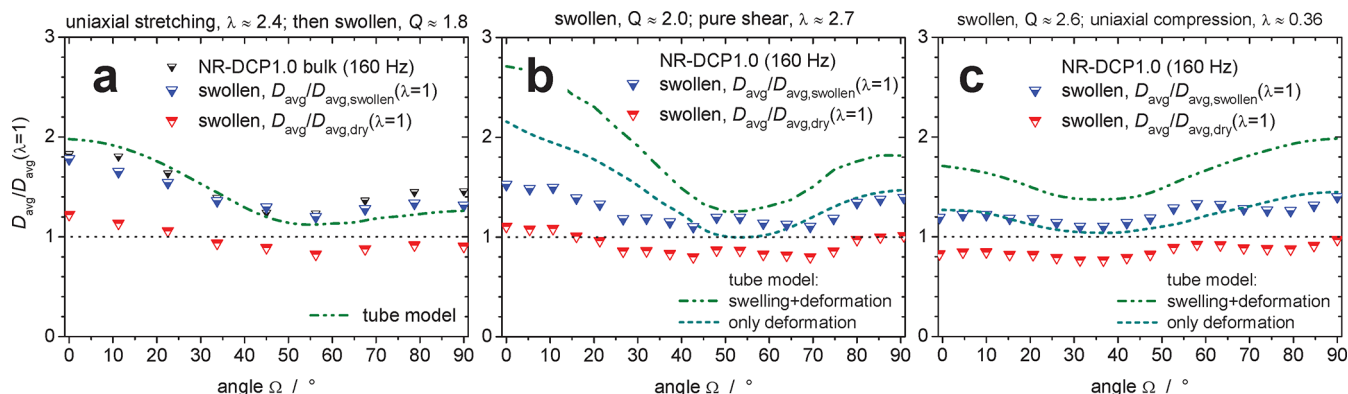
Figure 5. Orientation-dependent normalized average residual couplings for various NR and BR samples and three types of deformation: (a) uniaxial stretching, (b) pure-shear deformation, and (c) uniaxial compression. Each panel shows predictions from the three models considered, finding in every case best agreement with the phantom and tube models. For every sample $D_{avg}/2\pi$ reflecting its cross-link density is given in brackets.
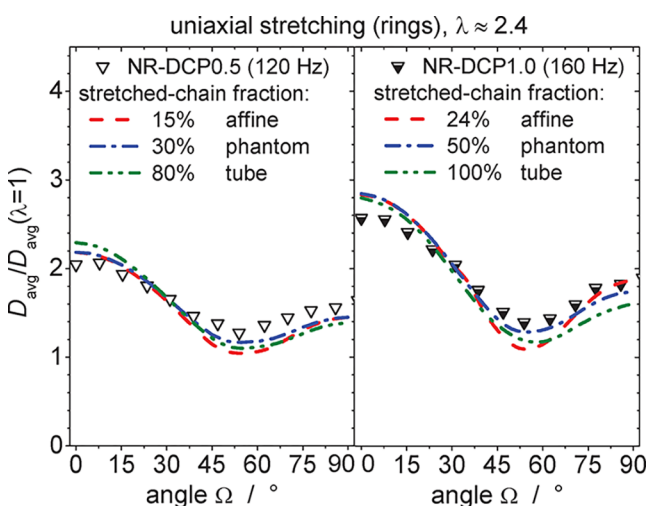
Figure 6. Orientation-dependent normalized average residual couplings for two uniaxially stretched NR samples ($\lambda \approx 2.4$), fitted to all three models assuming a variable fraction of unstretched, thus nonoriented chains. The relative amount of deformed chains is indicated, and $D_{avg}/2\pi$ values reflecting the cross-linking density are given in brackets.

anisotropic swelling, i.e., simultaneous swelling and deformation. For the first two options we can treat both deformations separately, as the order of the two steps should not matter (because the deformation matrixes are diagonal). Then, one point of consideration is that in the dry and swollen states the end-to-end distances before anisotropic deformation (R_0) are not the same: $R_{0,dry} < R_{0,sw}$. This difference can be easily accounted for by a change in normalization for D_{avg} for mechanically deformed samples to dry- or swollen-state values, respectively, of D_{avg} for $\lambda = 1$.

Figure 7a−c collects data along these lines for one sample. Panel (a) shows the case of stretched rubber rings that were afterward swollen; we remind that the range of accessible λ and in particular Q values is rather limited in this case, due to a lack of mechanical integrity of the samples. It is noticed that the swollen-state data closely matches the data for the same stretched sample before swelling once the data are normalized accordingly. This indicates that at the given moderate $Q = 1.8$, swelling of the stretched polymer network (resulting in a $\lambda_Q = \sqrt[3]{Q} \approx 1.2$) does not change the average relative configuration of the prestretched network chains. At the same time, though, swelling does lead to a considerable broadening of the D_{res} distribution (data not shown), meaning that the network reorganizes considerably.

Figure 7. Orientation-dependent normalized average residual couplings for sample NR-DCP1.0 exploring swelling effects in DBS. (a) Swelling of a uniaxially stretched sample, (b) pure-shear deformation and (c) uniaxial compression of swollen samples. The results are normalized with respect to both the dry-state and swollen-state D_{avg} values in the unstretched state. In (a) the same angular dependency as before swelling is observed for the latter case. In (b) and (c), simulation results for the tube model are shown, including or excluding the swelling as an active deformation.

Figure 7b,c shows data and simulation results for the deformation of preswollen rubbers in pure shear and uniaxial compression, respectively. Again, experimental data are normalized to the dry as well as swollen states. The experimental angle variation is rather weak, weaker than for any of our models. That is the reason why we restrict the simulations to tube-model predictions. The simulations follow the deformation matrices given by eqs 5 and 6 for compression and pure shear, respectively. In all cases, predictions overestimate the experimental microscopic deformation in both magnitude and angular dependence. We also include simulations where the macroscopic swelling-expansion step is excluded, using $Q = 1$ vs the actual Q in eqs 5,6. These results, which exclude the swelling-related deformation, are expected to better describe the experimental D_{avg} when they are normalized to the isotropical swollen-state value at $\lambda = 1$. The fits of the corresponding data are indeed considerably better.

As to higher degrees of swelling further beyond the initial desinterspersion stage (where affine deformation dominates for isotropic dilation), we were not able to gather enough data for a reliable angular variation. We can, however, discuss an angle-averaged value of $D_{avg}/D_{avg,swollen}(\lambda = 1)$ for sample NR-DCP0.5 for $Q \approx 5$ at $\lambda \approx 2.25$ in pure shear. We obtained 1.05 ± 0.1, to be compared with 1.95, 1.7, and 1.13 expected for the affine, phantom and tube models, respectively. Clearly, also in this case the affine and phantom predictions are not compatible with the data, and even the tube model prediction is on the large side.

Finally, we turn to the case of uniaxial swelling in a fixed sample tube, which avoids the noted problems with mechanical integrity and thus allows for effectively larger Q values, well in the desinterspersed, nominally isotropic-affine range. For the data see Figure 4b, right panel. As a down side, though, both $D_{avg}(\Omega)$ as well as the actual Q are subject to larger uncertainty, owing to the small sample size and shape, respectively.

In rationalizing the data collected in Figure 8, we have again two options, i.e., considering the final state to arise from a deformation of a nonswollen vs a preswollen sample. In the former case it is assumed that during swelling chains of the sample are stretching during expansion as described by eq 7, i.e., $\lambda_z = Q$, meaning that we assume the absence of entanglement/packing effects. The experimental data should in this case be normalized to be back-extrapolated $D_{res,c}$ value representing the elastic chains active in the swollen state, but in a state of stretching corresponding to the dry state (we refer to this as "non-swollen" initial state). This certainly represents a limiting case, since entanglement effects are only reduced but not necessarily fully removed in the final state, and since the desinterspersion effect could proceed differently in uniaxially vs isotropically swollen samples. Data for this case are compared in Figure 8a, and they are seen to cluster around the phantom model prediction.

As the second possibility we can assume the isotropically swollen state to be the reference, in order to avoid making assumptions on the complexities of the structural unfolding process during swelling. This is probably the more realistic standpoint, and it means we should normalize the experimental data to the value in the isotropically swollen state at the same Q value. In order to calculate the corresponding model predictions, we need to decompose the deformation matrix, eq
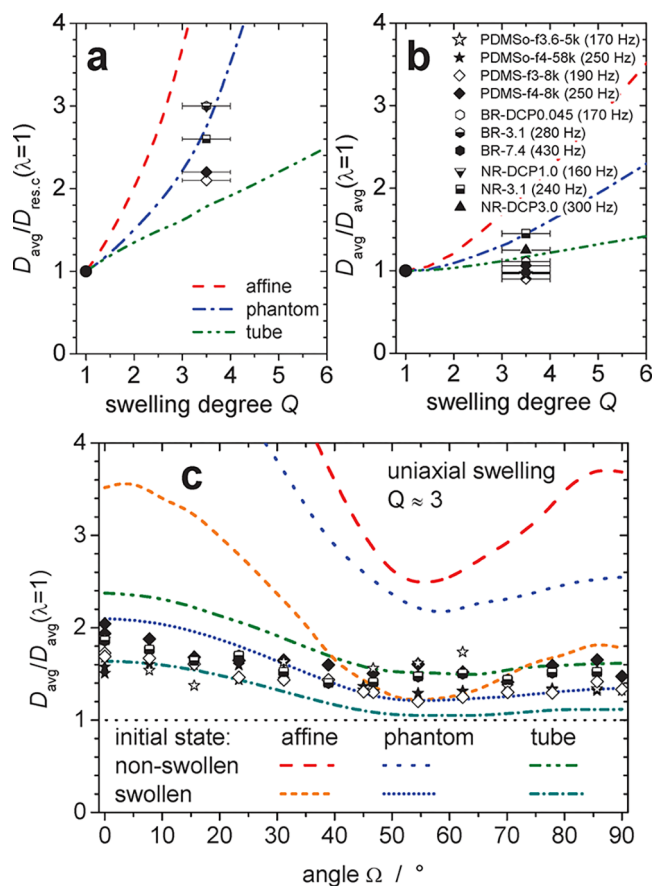
Figure 8. Normalized average residual couplings for various NR, BR, and PDMS samples swollen uniaxially in d-toluene. Panels (a) and (b) show the powder-averaged results for the investigated degree of swelling of $Q \approx 3.5$ in comparison to simulations as a function of Q, taking (a) the back-extrapolated "non-swollen" $D_{avg,c}$ and (b) the isotropic swollen-state D_{avg} as reference. (c) Orientation-dependent results along with simulations.

7, into a product of two matrices describing separate isotropic dilation (swelling) and uniaxial deformation:

$$\Lambda_{us} = \begin{pmatrix} \sqrt[3]{Q} & 0 & 0 \\ 0 & \sqrt[3]{Q} & 0 \\ 0 & 0 & \sqrt[3]{Q} \end{pmatrix} \times \begin{pmatrix} \dfrac{1}{\sqrt[3]{Q}} & 0 & 0 \\ 0 & \dfrac{1}{\sqrt[3]{Q}} & 0 \\ 0 & 0 & \sqrt[3]{Q^2} \end{pmatrix}$$

(19)

In this case we have an effective uniaxial elongation by $\lambda_z = \sqrt[3]{Q^2}$ (with effective lateral shrinking by the square-root of this value). Since experimental data are normalized to the isotropically swollen state, we can neglect the first matrix in the simulations.

Looking at the data in Figure 8b, we see that all samples' results fall now well below the phantom prediction and cluster around the tube-model prediction. As to the angle dependence, Figure 8c, the phantom and tube models are not much different with regard to the overall angular variation, while the data for several rather different samples (randomly cross-linked vs endlinked) show even shallower dependencies around a somewhat elevated average value, matching the tube model at small and the phantom model at large angles.

To put all observations so far in perspective, we have seen that most of our results obtained on deformed swollen networks are best compatible with predictions of the tube model. We have, however, no good reason to justify such a treatment, as the model in the way as it is applied assumes the dominance of entanglement-related constraints. In its pure form it should neither be applicable to a bulk network dominated by chemical cross-links (which is the case for most of the studied samples), nor should it work in the swollen state. It remains to be concluded that the microscopic chain deformation in swollen networks appears to be dominated by spatial heterogeneity and complex topological rearrangements, resulting in rather weak overall orientation-dependent deformation, and thus angle dependence. The proximity to tube-model predictions should possibly be taken as fortuitous.

5.3. Defects in Swollen and Deformed Networks. The direct comparison of the local chain stretching in bulk vs swollen networks is subject to an uncertainty related to nonelastic defects. This fraction increases considerably upon swelling, mainly as a result of the partial release of entanglement and packing constraints.[7,36] In the bulk state, a part of the defects is entangled and potentially elastically active, either only transiently or even permanently through nematic interactions.[45,46,62,63] Therefore, it is important to state that in most of our samples the defect content is rather low, mostly below 10% except for the least-cross-linked samples (see Tables 1−3), and that it does not increase by more than about twice that value upon swelling.

Defects act as a diluent of entanglement constraints,[49] but since the defect fraction is moderate in most samples even in the swollen state, and since we see no systematic deviations between results for samples of variable cross-linking density and defect contents, we assume any related effect on our observations to be small. Importantly also, the fraction of network chains, for which the results of $D_{avg}(\Omega)$ are representative, does not change significantly upon swelling. Thus, our results always reflect the average (=proton-number-averaged) behavior of a majority fraction of polymer segments.

An interesting aspect in this context is the stretching and angle dependence of the defect fraction. In our previous work[37] we already found that bulk stretched samples exhibit apparently less defects, and that the defect fraction is maximal at the magic-angle orientation ($\Omega = 54.7°$). This is in tune with the concept of nematic interactions,[45,46] which should vanish at that orientation due to the dependence following the second Legendre polynomial, $P_2(\cos \Omega)$. Figure 9 collects such results for uniaxially swollen samples, where the use of deuterated toluene allowed for an assessment of the defect fraction (yet compromised by the poor signal due to small samples).

On the whole, we see a significant trend toward lower apparent defect fractions in the stretched vs the unstretched swollen samples. There is also a rather weak, hardly significant trend toward larger defect fractions in the 45° angle range. This finding is overall surprising, because nematic interactions, which arise from next-neighbor packing, should be largely absent or at least significantly reduced in the swollen state. Therefore, we can assume that isotropically moving defects could also be related to loop structures, where the close ends of the loop can be removed from each other by deformation of the swollen sample. We can take this as another indication of rather significant reorganization going on in a swollen sample upon further deformation. Such processes, leading to low effective orientation, are well in line with computer simulations
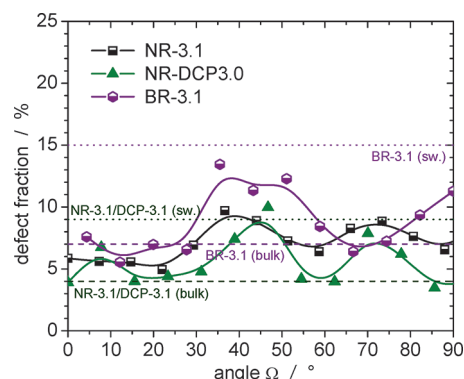
Figure 9. Defect fraction of selected uniaxially swollen samples as a function of orientation. The defect contents in the dry and isotropically swollen states are indicated as dashed and dotted lines, respectively.

of topologically realistic networks[64] and "olympic gels," i.e., permanently entangled ring polymers.[47]

6. CONCLUSIONS

In this work, we have investigated the microscopic deformation of polymer network chains in samples of widely variable cross-linking density upon swelling and mechanical deformation beyond the linear range. We have used proton multiple-quantum NMR to measure static orientation correlations of chain segments, as quantified by an average residual dipolar coupling (RDC), which directly reflects the end-to-end distances R. Our method allows for the assessment of the distribution function of RDCs, which has a significant width owing to swelling inhomogeneities and orientation-dependent stretching. We have devised a reliable data analysis procedure to quantify a proper average RDC as a function of sample orientation with respect to the magnetic field, and compare it with predictions from simulations based upon the affine, phantom, and tubes model of rubber elasticity.

We have performed such a comparison for three types of deformation: uniaxial stretching, compression, and pure shear, as applied to dry as well as swollen rubbers of different kinds, thus stressing the generality of our findings. All data are indicating a rather weak average microscopic stretching of the network chains, and a correspondingly weak angle dependence. We have shown that this can also be explained by a heterogeneous scenario, i.e., a coexistence of a more strongly stretched subensemble and a significant fraction of non-deformed and nonoriented chains. Excluding such a possibility, the data fall well below the affine prediction, even below the phantom-model prediction, and is thus on average closest to that of the tube model. This is the case even for highly cross-linked rubbers and swollen samples, where entanglement constraints are less relevant. It is the subject of ongoing work to clarify the influence of entanglement constraints as a function of the degree of swelling.

We conclude that the microscopic deformation in swollen networks, possibly even in bulk networks, is governed by a significant reorganization and the appearance of heterogeneities once going beyond the linear deformation range. Similar conclusions were recently drawn from results of computer simulations of entangled long-chain melts.[65] In this light, the applicability of any chain-based mean-field-type model that ignores structural heterogeneity and the resulting topological rearrangements appears questionable. This includes all tube

models that are discussed with regard to nonlinear deformation.

■ AUTHOR INFORMATION

Corresponding Author

*E-mail: kay.saalwaechter@physik.uni-halle.de; URL: www.physik.uni-halle.de/nmr.

ORCID ⓘ

Juan Lopez Valentin: 0000-0002-3916-9060
Kay Saalwächter: 0000-0002-6246-4770

Notes

The authors declare no competing financial interest.

■ REFERENCES

(1) Treloar, L. R. G.; Montgomery, D. J. The Physics of Rubber Elasticity. *Phys. Today* **1959**, *12*, 32−34.

(2) Erman, B.; Mark, J. E. Rubber-Like Elasticity. *Annu. Rev. Phys. Chem.* **1989**, *40*, 351−374.

(3) Guth, E.; James, H. M. Elastic and Thermoelastic Properties of Rubberlike Materials. *Ind. Eng. Chem.* **1941**, *33*, 624−629.

(4) Erman, B. Chain dimensions in deformed networks: theory and comparison with experiment. *Macromolecules* **1987**, *20*, 1917−1924.

(5) Ullman, R. Small-angle neutron scattering from elastomeric networks. Application to labeled chains containing several crosslinks. *Macromolecules* **1982**, *15*, 1395−1402.

(6) Callaghan, P. T.; Samulski, E. T. Biaxial Deformation of a Polymer Network Measured via Deuteron Quadrupolar Interactions. *Macromolecules* **2003**, *36*, 724−735.

(7) Valentín, J. L.; Carretero-González, J.; Mora-Barrantes, I.; Chassé, W.; Saalwächter, K. Uncertainties in the Determination of Cross-Link Density by Equilibrium Swelling Experiments in Natural Rubber. *Macromolecules* **2008**, *41*, 4717−4729.

(8) Chassé, W.; Lang, M.; Sommer, J.-U.; Saalwächter, K. Cross-Link Density Estimation of PDMS Networks with Precise Consideration of Networks Defects. *Macromolecules* **2012**, *45*, 899−912 Correction ; *Macromolecules* **2015**, *48*, 1267−1268.

(9) Akagi, Y.; Katashima, T.; Katsumoto, Y.; Fujii, K.; Matsunaga, T.; Chung, U.-i.; Shibayama, M.; Sakai, T. Examination of the Theories of Rubber Elasticity Using an Ideal Polymer Network. *Macromolecules* **2011**, *44*, 5817−5821.

(10) Akagi, Y.; Gong, J. P.; Chung, U.; Sakai, T. Transition between Phantom and Affine Network Model Observed in Polymer Gels with Controlled Network Structure. *Macromolecules* **2013**, *46*, 1035−1040.

(11) Lange, F.; Schwenke, K.; Kurakazu, M.; Akagi, Y.; Chung, U.; Lang, M.; Sommer, J.-U.; Sakai, T.; Saalwächter, K. Connectivity and Structural Defects in Model Hydrogels: A Combined Proton NMR and Monte Carlo Simulation Study. *Macromolecules* **2011**, *44*, 9666−9674.

(12) Zhou, H.; Woo, J.; Cok, A. M.; Wang, M.; Olsen, B. D.; Johnson, J. A. Counting primary loops in polymer gels. *Proc. Natl. Acad. Sci. U. S. A.* **2012**, *109*, 19119−19124.

(13) Zhong, M.; Wang, R.; Kawamoto, K.; Olsen, B. D.; Johnson, J. A. Quantifying the impact of molecular defects on polymer network elasticity. *Science* **2016**, *353*, 1264−1268.

(14) Biswas, S.; Yashin, V. V.; Balazs, A. C. Patterning with loops" to dynamically reconfigure polymer gels. *Soft Matter* **2018**, *14*, 3361−3371.

(15) de Gennes, P. G. Reptation of a Polymer Chain in the Presence of Fixed Obstacles. *J. Chem. Phys.* **1971**, *55*, 572−579.

(16) Doi, M.; Edwards, S. F. Dynamics of concentrated polymer systems. Part 1.—Brownian motion in the equilibrium state. *J. Chem. Soc., Faraday Trans. 2* **1978**, *74*, 1789−1801.

(17) Edwards, S. F.; Vilgis, T. A. The tube model theory of rubber elasticity. *Rep. Prog. Phys.* **1988**, *51*, 243−297.

(18) McLeish, T. C. B. Tube theory of entangled polymer dynamics. *Adv. Phys.* **2002**, *51*, 1379−1527.

(19) Gottlieb, M.; Gaylord, R. J. Experimental tests of entanglement models of rubber elasticity: 1. Uniaxial extension-compression. *Polymer* **1983**, *24*, 1644−1646.

(20) Gottlieb, M.; Gaylord, R. J. Experimental tests of entanglement models of rubber elasticity. 2. Swelling. *Macromolecules* **1984**, *17*, 2024−2030.

(21) Gottlieb, M.; Gaylord, R. J. Experimental tests of entanglement models of rubber elasticity. 3. Biaxial deformations. *Macromolecules* **1987**, *20*, 130−138.

(22) Heinrich, G.; Straube, E.; Helmis, G. Rubber Elasticity of Polymer Networks − Theories. *Adv. Polym. Sci.* **1988**, *85*, 33−87.

(23) Rubinstein, M.; Panyukov, S. Nanaffine Deformation and Elasticity of Polymer Networks. *Macromolecules* **1997**, *30*, 8036−8044.

(24) Urayama, K.; Kawamura, T.; Kohjiya, S. Multiaxial Deformations of End-linked Poly(dimethylsiloxane) Networks. 2. Experimental Tests of Molecular Entanglement Models of Rubber Elasticity. *Macromolecules* **2001**, *34*, 8261−8269.

(25) Basterra-Beroiz, B.; Rommel, R.; Kayser, F.; Westermann, S.; Valentin, J. L.; Heinrich, G. Swelling of polymer networks with topological constraints: Application of the Helmis-Heinrich-Straube model. *eXPRESS Polym. Lett.* **2018**, *12*, 731−739.

(26) Beltzung, M.; Picot, C.; Herz, J. Investigation of the Chain Conformation in Uniaxially Stretched Poly(dimethylsiloxane) Networks by Small-Angle Neutron Scattering). *Macromolecules* **1984**, *17*, 663−669.

(27) Hild, G. Model networks based on 'endlinking' processes: synthesis, structure and properties. *Prog. Polym. Sci.* **1998**, *23*, 1019−1149.

(28) Westermann, S.; Pyckhout-Hintzen, W.; Richter, D.; Straube, E.; Egelhaaf, S.; May, R. On the Length Scale Dependence of Microscopic Strain by SANS. *Macromolecules* **2001**, *34*, 2186−2194.

(29) Pyckhout-Hintzen, W.; Westermann, S.; Wischnewski, A.; Monkenbusch, M.; Richter, D.; Straube, E.; Farago, B.; Lindner, P. Direct Observation of Nonaffine Tube Deformation in Strained Polymer Networks. *Phys. Rev. Lett.* **2013**, *110*, 196002.

(30) Mallam, S.; Horkay, F.; Hecht, A.-M.; Rennie, A. R.; Geissler, E. Microscopic and Macroscopic Thermodynamic Observations in Swollen Poly(dimethylsiloxane) Networks. *Macromolecules* **1991**, *24*, 543−548.

(31) Mendes, E., Jr.; Lindner, P.; Buzier, M.; Boué, F.; Bastide, J. Experimental Evidence for Inhomogenious Swelling and Deformation in Statistical Gels. *Phys. Rev. Lett.* **1991**, *66*, 1595−1598.

(32) Matsunaga, T.; Asai, H.; Akagi, Y.; Sakai, T.; Chung, U.; Shibayama, M. SANS Studies on Tetra-PEG Gel under Uniaxial Deformation. *Macromolecules* **2011**, *44*, 1203−1210.

(33) Saalwächter, K. Proton Multiple-Quantum NMR for the Study of Chain Dynamics and Structural Constraints in Polymeric Soft Materials. *Prog. Nucl. Magn. Reson. Spectrosc.* **2007**, *51*, 1−35.

(34) Saalwächter, K. Robust NMR Approaches for the Determination of Homonuclear Dipole−Dipole Coupling Constants in Studies of Solid Materials and Biomolecules. *ChemPhysChem* **2013**, *14*, 3000−3014.

(35) Saalwächter, K.; Kleinschmidt, F.; Sommer, J.-U. Swelling Heterogeneities in End-Linked Model Networks: A Combined Proton Multiple-Quantum NMR and Computer Simulation Study. *Macromolecules* **2004**, *37*, 8556−8568.

(36) Chassé, W.; Schlögl, S.; Riess, G.; Saalwächter, K. Inhomogeneities and local chain stretching in partially swollen networks. *Soft Matter* **2013**, *9*, 6943−6954.

(37) Ott, M.; Pérez-Aparicio, R.; Schneider, H.; Sotta, P.; Saalwächter, K. Microscopic Study of Chain Deformation and Orientation in Uniaxially Strained Polymer Networks: NMR Results versus Different Network Models. *Macromolecules* **2014**, *47*, 7597–7611.

(38) Pérez-Aparicio, R.; Schiewek, M.; Valentín, J. L.; Schneider, H.; Long, D. R.; Saphiannikova, M.; Sotta, P.; Saalwächter, K.; Ott, M. Local Chain Deformation and Overstrain in Reinforced Elastomers: An NMR Study. *Macromolecules* **2013**, *46*, 5549–5560.

(39) Saalwächter, K.; Sommer, J.-U. NMR Reveals Non-Distributed and Uniform Character of Network Chain Dynamics. *Macromol. Rapid Commun.* **2007**, *28*, 1455–1465.

(40) Deloche, B.; Samulski, E. T. Short-Range Nematic-like Orientational Order in Strained Elastomers: A Deuterium Magnetic Resonance Study. *Macromolecules* **1981**, *14*, 575–581.

(41) Gronski, W.; Stadler, R.; Jacobi, M. M. Evidence of nonaffine and inhomogeneous deformation of network chains in strained rubber-elastic networks by deuterium magnetic resonance. *Macromolecules* **1984**, *17*, 741–748.

(42) Sotta, P.; Deloche, B.; Herz, J.; Lapp, A.; Durand, D.; Rabadeux, J. C. Evidence for short-range orientational couplings between chain segments in strained rubbers: a deuterium magnetic resonance investigation. *Macromolecules* **1987**, *20*, 2769–2774.

(43) Hedden, R. C.; McCaskey, E.; Cohen, C.; Duncan, T. M. Effects of Molecular Structure on Segment Orientation in Siloxane Elastomers. 1. NMR Measurements from Compressed Samples. *Macromolecules* **2001**, *34*, 3285–3293.

(44) Kuhn, W.; Grün, F. Beziehungen zwischen elastischen Konstanten und Dehnungsdoppelbrechung hochelastischer Stoffe. *Colloid Polym. Sci.* **1942**, *101*, 248–271.

(45) Ylitalo, C. M; Zawada, J. A; Fuller, G. G; Abetz, V.; Stadler, R. Oligomers as molecular probes of orientational coupling interactions in polymer melts and networks. *Polymer* **1992**, *33*, 2949–2960.

(46) Shetty, S.; Gomez, E. D.; Milner, S. T. Nematic Coupling in Polybutadiene from MD Simulations. *Macromolecules* **2019**, *52*, 528–534.

(47) Qin, J.; So, J.; Milner, S. T. Tube Diameter of Stretched and Compressed Permanently Entangled Polymers. *Macromolecules* **2012**, *45*, 9816–9822.

(48) Valentín, J. L.; Posadas, P.; Fernández-Torres, A.; Malmierca, M. A.; González, L.; Chassé, W.; Saalwächter, K. Inhomogeneities and Chain Dynamics in Diene Rubbers Vulcanized with Different Cure Systems†. *Macromolecules* **2010**, *43*, 4210–4222.

(49) Campise, F.; Agudelo, D. C.; Acosta, R. H.; Villar, M. A.; Vallés, E. M.; Monti, G. A.; Vega, D. A. Contribution of Entanglements to Polymer Network Elasticity. *Macromolecules* **2017**, *50*, 2964–2972.

(50) Saalwächter, K.; Ziegler, P.; Spyckerelle, O.; Haidar, B.; Vidal, A.; Sommer, J.-U. ^{1}H multiple-quantum nuclear magnetic resonance investigations of molecular order distributions in poly-(dimethylsiloxane) networks: Evidence for a linear mixing law in bimodal systems. *J. Chem. Phys.* **2003**, *119*, 3468–3482.

(51) Kovermann, M.; Saalwächter, K.; Chassé, W. Real-Time Observation of Polymer Network Formation by Liquid- and Solid-State NMR Revealing Multistage Reaction Kinetics. *J. Phys. Chem. B* **2012**, *116*, 7566–7574.

(52) Baum, J.; Pines, A. NMR Studies of Clustering in Solids. *J. Am. Chem. Soc.* **1986**, *108*, 7447–7454.

(53) Sommer, J.-U.; Chassé, W.; Valentín, J. L.; Saalwächter, K. Effect of excluded volume on segmental orientation correlations in polymer chains. *Phys. Rev. E* **2008**, *78*, 051803.

(54) Weese, J. A reliable and fast method for the solution of Fredhol integral equations of the first kind based on Tikhonov regularization. *Comput. Phys. Commun.* **1992**, *69*, 99–111.

(55) Chassé, W.; Valentín, J. L.; Genesky, G. D.; Cohen, C.; Saalwächter, K. Precise dipolar coupling constant distribution analysis in proton multiple-quantum NMR of elastomers. *J. Chem. Phys.* **2011**, *134*, 044907.

(56) Naumova, A.; Tschierske, C.; Saalwächter, K. Orientation-dependent proton double-quantum NMR build-up function for soft materials with anisotropic mobility. *Solid State Nucl. Magn. Reson.* **2017**, *82–83*, 22–28.

(57) Pearson, D. Scattered Intensity from a Chain in a Rubber Network. *Macromolecules* **1977**, *10*, 696–701.

(58) Wagner, M. H. Analysis of Small-Angle Neutron Scattering Data on Poly(dimethylsiloxane) Network Unfolding. *Macromolecules* **1994**, *27*, 5223–5226.

(59) Basterra-Beroiz, B.; Rommel, R.; Kayser, F.; Valentín, J. L.; Westermann, S.; Heinrich, G. Revisiting Segmental Order: A Simplified Approach for Sulfur-Cured Rubbers Considering Junction Fluctuations and Entanglements. *Macromolecules* **2018**, *51*, 2076–2088.

(60) Saalwächter, K.; Herrero, B.; López-Manchado, M. A. Chemical Shift-Related Artifacts in NMR Determinations of Proton Residual Dipolar Couplings in Elastomers. *Macromolecules* **2005**, *38*, 4040–4042.

(61) Mark, J. E., Ed. *Physical Properties of Polymers Handbook*; Springer: New York, 2007.

(62) Jarry, J.-P.; Monnerie, L. Effects of Nematic-Like Interaction in Rubber Elasticity Theory. *Macromolecules* **1979**, *12*, 316–320.

(63) Deloche, B.; Samulski, E. T. Rubber Elasticity: A Phenomenological Approach Including Orientational Correlations. *Macromolecules* **1988**, *21*, 3107–3111.

(64) Hölzl, T.; Trautenberg, H. L.; Göritz, D. Monte Carlo Simulations on Polymer Network Deformation. *Phys. Rev. Lett.* **1997**, *79*, 2293–2296.

(65) Hsu, H.-P.; Kremer, K. Primitive Path Analysis and Stress Distribution in Highly Strained Macromolecules. *ACS Macro Lett.* **2018**, *7*, 107–111.